APPLICATIONS OF SH MODE FOR MEASUREMENT OF ANISOTROPIC PROPERTIES OF SOLIDS

Kwang Yul Kim, A. Richard Baker, and Wolfgang Sachse
Department of Theoretical and Applied Mechanics
Cornell University
Ithaca, New York 14853, USA

Arthur G. Every
Department of Physics
University of the Witwatersrand
Johannesburg, South Africa

INTRODUCTION

Shear-horizontally (SH) polarized transverse (T) modes are uncoupled from the longitudinal (L) (quasilongitudinal (QL)) mode and transverse (quasitransverse (QT)) mode of shear-vertical (SV) polarization, which are generally coupled with each other. This offers certain advantages to using the SH modes for investigation of the phenomena related to the arrivals of transverse modes, because their arrival and amplitude are not affected by the preceding arrivals of the L (QL) modes and the head waves (HW) in some directions and therefore can be clearly identified and measured in the signal generated by a small pointlike source (PS). In this work the SH modes propagating inside a specimen are generated using a pointlike or a line-segment shear (S) mode piezoelectric $Pb(Zr,Ti)O_3$ (PZT) transducer attached on the surface of a (001)-oriented cubic silicon disk, a (001)-oriented transversely isotropic zinc disk, and a thin orthorhombic poly ether ether kethon (PEEK) composite plate oriented in a principal symmetry plane. The SH modes are detected on the surface of the specimen by a pointlike S mode PZT detector which is polarized in the same direction as the source transducer. A novel technique using the SH modes for measurements of shear elastic moduli, such as C_{44}, C_{55}, and C_{66}, is presented for all these specimens. Investigated also using the SH modes is a focusing of fast transverse (FT) modes in silicon. The focusing pattern in silicon is in sharp contrast to the SH mode radiation pattern observed in an isotropic glass plate.

THEORY

Elastodynamic Green's Functions

A time domain displacement response $G_{kl}(\underline{x},t)$ in the x_k direction at a position $\underline{x}$ in an infinite elastic continuum to a concentrated point force acting in the x_l direction at origin with Heaviside step function time dependence $\Theta(t)$ can be expressed in the form [1]

$$G_{kl}(\underline{x},t)=\sum_{n=1}^{3}\left\{\frac{-1}{8\pi^2\rho}\int_{\Omega} d\Omega\, s^{(n)3}\Lambda_{kl}^{(n)}\,\delta\left(t-\underline{s}^{(n)}\cdot\underline{x}\right)+\frac{\Theta(t)}{8\pi^2\rho x}\int_0^{2\pi} d\varphi\, s^{(n)2}\Lambda_{kl}^{(n)}\right\}, \qquad (1)$$

Review of Progress in Quantitative Nondestructive Evaluation, Vol. 15
Edited by D.O. Thompson and D.E. Chimenti, Plenum Press, New York, 1996

which in frequency domain can be written as

$$\tilde{G}_{kl}(\underline{x},\omega)=\sum_{n=1}^{3}\left\{\frac{i\omega}{8\pi^2\rho}\int_{\Omega}d\Omega\, s^{(n)3}\Lambda_{kl}^{(n)}\, e^{i\omega\underline{s}^{(n)}\cdot\underline{x}}+\frac{1}{8\pi^2\rho x}\int_{0}^{2\pi}d\varphi\, s^{(n)2}\Lambda_{kl}^{(n)}\right\}. \qquad (2)$$

The sum in Eqs. (1) and (2) is taken over the three acoustic branches. ρ, $d\Omega$, and φ denote the density of the medium, an element of the solid angle in which the slowness vector $\underline{s}$ lies, and a polar spherical angle, respectively. The first integral is a surface integral taken over the unit forward hemisphere centered on the observation direction and the second one is a line integral taken around the periphery of this hemisphere. The Green's functions G_{kl} and $\tilde{G}_{kl}$ depends, through the factor $\Lambda_{kl}^{(n)}=U_k^{(n)}U_l^{(n)}$, on the projection of the polarization vector $\underline{U}^{(n)}$ of each mode on the forcing and sensing directions.

Wave arrival singularities in the displacement response arise from integration over points on the slowness surface where $\underline{s}\cdot\underline{x}$ is stationary, i.e., where the normal to the slowness surface or group velocity points in the direction of a detector position $\underline{x}$. At the wave arrivals of various modes $G_{kl}(\underline{x},t)$ exhibits singular features, such as discontinuity, kink, and logarithmic or power law divergence, etc. They propagate outwards from the source at group velocities in any direction and collectively lie on the wave surface, which is the group velocity surface scaled in size by a factor t. These wave arrival features are discussed in detail by Every and Kim [1].

Identification of SH Mode Arrival and Shear Moduli

Let's denote three principal directions of orthorhombic symmetry by x_1, x_2, and x_3 axes. Of particular relevance to the study of the SH mode is the behavior of $G_{11}(\underline{x},t)$ and $G_{22}(\underline{x},t)$ observed respectively in the x_2x_3 and x_1x_3 symmetry planes for specimens of disk or plate shape oriented in the plane normal to x_3 axis. They can be easily generated on the specimen surface by aligning the polarization of the S-mode PZT transducer along either x_1 or x_2 direction. Since understanding one of them implies the understanding of the other, let pay our attention to $G_{11}(\underline{x},t)$. From symmetry argument, no sagittal component of a displacement can be present in the x_2x_3 plane, and therefore $G_{11}(\underline{x},t)$ in the x_2x_3 plane is a SH polarized pure transverse (PT) wave.

Among the SH modes of wide frequency spectrum generated by the PZT source, those below the cutoff frequencies are nonpropagating and thus tend to localize. These nonpropagating SH modes could be used to evaluate the quality of local flaws. In this work, however, we are interested in propagating SH modes with real wave numbers. We restrict ourselves to a specimen of orthorhombic or higher symmetry. The elastic properties of a medium with orthorhombic symmetry can be characterized by nine elastic constants: C_{11}, C_{22}, C_{33}, C_{12}, C_{13}, C_{23}, C_{44}, C_{55}, and C_{66}. The behavior of $G_{11}(\underline{x},t)$ in the x_2x_3 plane is described in Ref. 1. The first arrival is characterized as a weak kink caused by the QL mode arrival in the immediate neighborhood of the x_2x_3 plane. Inside the cuspidal region, following the QL mode arrival, one branch of the QT mode may arrive earlier than the PT wave of SH polarization, causing a kink in waveform. Outside the cuspidal region the SH mode arrives after the QL mode. Whether within the cuspidal region or not, the arrival of the SH PT mode causes a discontinuity, causing a big swing in waveform and thus facilitating its identification as the SH polarized PT arrival. The effects of the QL and QT arrivals fall off with $1/x^2$, being characterized as the near field effects, and can be observed with relatively thin specimen. In the far field, however, they may be buried in the noise and it may be the SH mode that is observed to arrive first above the noise level of the signal.

The SH wave propagating with group velocity V_g in the symmetry plane, say the x_2x_3 plane at an angle ζ to the x_3 axis, satisfies the relation [2]

$$\left(\rho V_g\right)^{-1} = \left(C_{55}\right)^{-1}\cos^2\zeta + \left(C_{66}\right)^{-1}\sin^2\zeta, \tag{3}$$

which indicates that two shear moduli C_{55} and C_{66} can be obtained by measuring the group velocities at least in two different directions. By performing similar experiments in the x_1x_2 and x_1x_3 planes all shear moduli C_{44}, C_{55} and C_{66} can be determined from measurements of SH mode group velocities. For transversely isotropic medium, $C_{11} = C_{22}$, $C_{13} = C_{23}$, $C_{44} = C_{55}$, and $C_{66} = (C_{11} - C_{12})/2$; for a cubic medium, $C_{11} = C_{22} = C_{33}$, $C_{12} = C_{23} = C_{13}$, and $C_{44} = C_{55} = C_{66}$; for an isotropic material, $C_{44} = (C_{11} - C_{12})/2$ in addition to those that hold in cubic symmetry, and two Lame constants $\lambda = C_{12}$ and $\mu = C_{44}$ are often used to characterize its elastic behavior.

Focusing of Fast Transverse Modes in Silicon

In silicon the fast transverse modes are PT as well as SH in the {100} planes and {110} planes out to the <111> directions, Between these two set of planes the polarization patterns for the FT modes are nearly SH [3]. The FT mode focusing pattern based on geometrical acoustics is plotted in Figure 1(a), which is generated using a Monte Carlo scheme, based on the assumption of a uniform distribution of wave normals in all directions. The focusing is confined in the narrow bands about the {100} planes, bounded by a pair of caustics that straddle these planes and converge on the <100> directions. Fig. 1(a) is in excellent agreement with the observed focusing of ballistic phonons at 2 °K [4].

At very high frequencies $\tilde{G}_{kl}(\underline{x}, \omega)$ in Eq. (2) can be analytically approximated, resulting in

$$\tilde{G} \approx \Lambda e^{i\omega \underline{\mathbf{s}}\cdot\underline{x}} / \sqrt{L_1 L_2}, \tag{4}$$

where L_1 and L_2 are the two principal curvatures of the slowness surface. The intensity or energy flux contributed from each frequency band is proportional to $\left|\tilde{G}\right|^2$ and is thus inversely proportional to $|K| = |L_1L_2|$, where K is the Gaussian curvature. The points of zero Gaussian curvature map into the caustics in Fig. 1(a). This result is precisely predicted on the basis of geometrical ray acoustics. [5]

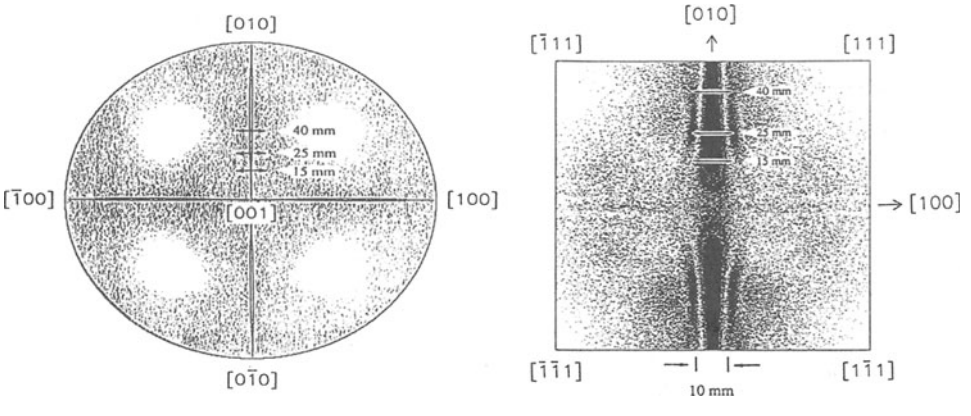

Figure 1. (a)Theoretical polar plot of the FT focusing pattern in silicon based on geometrical acoustics and uniform distribution of wave normals. (b) Computed spatial variation of $\tilde{G}_{11}(\underline{x}, \omega)$ at 2 MHz on the $x_3 = 49.15$ mm plane. Three scan lines are indicated by bidirectional arrows in both figures.

For finite ωx corresponding to the ultrasonic frequencies used in our work, the focusing caustics unfold into Airy, Pearcey and higher order diffraction patterns, as evident in the observations by Weaver et al. [6] The FT mode caustics in silicon are diffraction broadened to the extent that they merge into a single broad ridge. Furthermore, the excitation in our experiment is directed in the [100] direction, which results in the strongest SH generation near the (100) plane and little excitation of the SH modes near the (010) plane. A striking consequence of this anisotropic distribution of wave normals is the suppression of the FT mode focusing near the (010) plane. Figure 1(b) shows the computed spatial variation of the Green's function component $\tilde{G}_{11}(\underline{x}, \omega)$ in the $x_3 = 49.15$ mm plane for $f = 2\pi\omega = 2$ MHz with darkness representing the magnitude of $\tilde{G}$; 49.15 mm is the thickness of the (001) oriented silicon specimen. As the frequency decreases from the very high value, the FT line caustics unfold into Airy diffraction patterns. The fringes broaden and eventually merge, becoming fewer in number as the frequency is further lowered. By 2 MHz only the central intense fringe and a single pair of side fringes are clearly evident. Fig. 1(b) is in broad agreement with our observations described in the next section.

EXPERIMENTAL RESULTS

The shear modulus C_{44} and focusing patterns of the FT modes which are almost nearly SH polarized are obtained with a (001) oriented silicon disk of 49. 15 mm thickness and 100 mm in diameter. The shear PZT source is polarized in the [100] direction and fixed at origin at the bottom face. The shear detector is polarized in the same direction as the source and scanned on the top surface. The area of excitation and sensing elements of the source and detector is a 0.75 mm diameter circle. At first the shear detector is scanned along the (100) plane passing through the source to measure SH mode group velocities in various directions in the (100) plane. A typical wave form obtained at a distance of 40 mm from epicenter is displayed in the x=0 mm graph of Figure 2. The detector positions satisfy the far-field condition. Therefore, the arrival times of the first signal above the noise level are those of the FT modes and used to calculate the SH polarized PT group velocities. These FT waves are all found to propagate with velocities nearly equal to $(C_{44}/\rho)^{1/2}$,

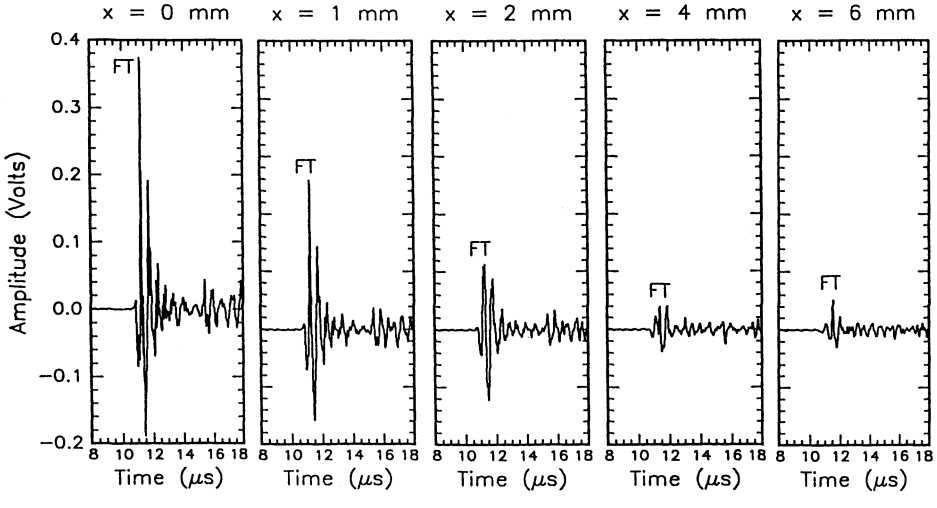

Figure 2. Observed waveforms at various positions on the scan line at 40 mm from epicenter.

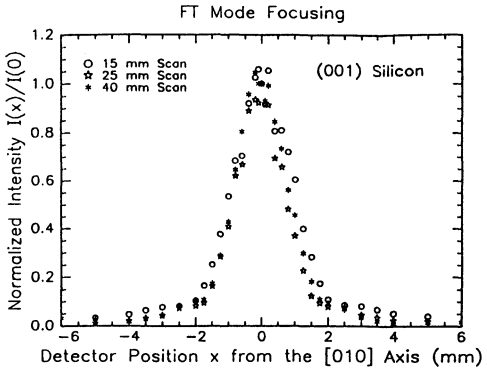

Figure 3. Observed FT mode focusing patterns in silicon near the (100) plane at 15, 25, and 40 mm scan lines.

regardless of their θ orientation. This is consistent with the (100) FT group velocity section described in Eq. (3). C_{44} obtained using the density of silicon, 2332 kg/m^3, is 79.56 GPa.

Next, FT focusing patterns are obtained by scanning the detector along three lines that intersect the same(100) plane at 15, 25 , and 40 mm away from the epicenter. The scan range is a 6 mm interval on either side of the (100) plane. Some of the waveforms obtained at the scan line of 40 mm away from the epicenter are displayed in Fig. 2, where the x value written on top of each waveform indicates the detector distance from the (100) plane. Note the rapid change in magnitude of the observed FT amplitude as the detector moves a small distance or a small φ from the (100) plane. The focusing behavior exhibited in Fig. 2 is illustrated in a graphical form in Figure 3, which shows normalized intensity $I(x)/I(0)$ as a function of x. The square of peak amplitude immediately after the arrival of the FT mode is used as a measure of intensity. The 2 mm half-width of the approximately Gaussian curve subtends an angle of 1.8°, when viewed from the source. Very similar focusing patterns are also obtained at 15 and 25 mm scan lines and plotted in the same Fig. 3. These narrow band focusing patterns are in good qualitative agreement with the behavior shown

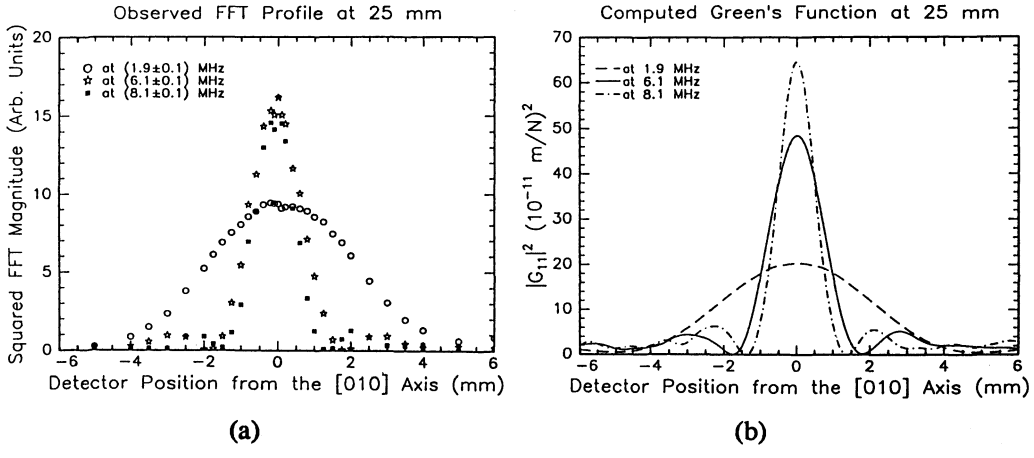

Figure 4. Variation of the squared modulus of Fourier components at 1.9, 6.1, and 8.1 MHz with at 25 mm scan line from epicenter: (a) observed and (b) computed.

in Fig. 1(a), which is obtained using geometrical acoustics. However, there are salient differences between these two figures. Fig. 1(a) indicates that the intensity is maximum (infinite) at the caustics, dipping to shallow minimum at the central (100) plane and goes to nearly zero immediately beyond the caustics, while Fig. 3 indicates a single intensity peak centered on the (100) plane. This is due to diffraction broadening at ultrasonic frequencies, which are the dominant frequencies of the observed signals.

To delve further, we consider individual Fourier components of the detected signals. All the detected signals are observed to have sharply peaked Fourier components at 1.9, 6.1, and 8.1 MHz. We take the case of the $|\tilde{G}_{11}(\underline{x},\omega)|^2$ at the 25 mm scan line. Figure 4 represents a detailed comparison between theory and experiment. Figure 4(a) shows the squared modulus of the 1.9, 6.1, and 8.1 MHz Fourier components of the observed waveforms as a function of a distance from the (100) plane, which compare well with the corresponding computed Green's functions shown in Figure 4(b). Only FT modes are included in the calculation. The calculated curves are in very good agreement with the observed Fourier components with regard to the widths and positions of the various peaks and minima. Similar agreements between theory and experiment are obtained for the other two scan lines at 15 and 25 mm. Moreover, the behaviors of the observed $|\tilde{G}_{11}(\underline{x},\omega)|^2$ at 1.9 MHz of the three scan lines are also in very good agreement with those in Fig. 2.

A SH mode radiation pattern in a isotropic glass plate of 25.5 mm thickness is obatined with a shear source fixed both in position and in polarization at origin on one side and a shear detector located at $\theta = 45°$ on the other side. θ is the cone angle of the spherical polar coordinates. We note here for clarity that the sagittal plane is defined by the normal to the glass plate and the source-to-detector direction. The source is polarized normal to the sagittal plane, while the detector polarization is rotated from $\varphi = -90°$ to $\varphi = 90°$ with this respect to this plane on the sample surface. Here φ is an angle between the normal to the sagittal plane and the polarization of the detector. This is equivalent to scanning the detector in a semicircle of radius 25.5 mm centered at the epicenter, while the detector polarization is maintained tangential to this circle or normal to the sagittal plane.

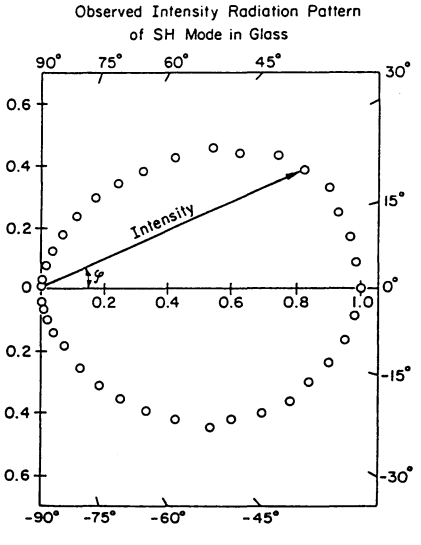

Figure 5. A polar plot of the observed SH mode intensity radiation pattern in glass.

The measurements yield the SH radiation pattern displayed in Figure 5, which shows the φ dependence of the SH intensity normalized with respect to the intensity at $\varphi = 0°$. The peak amplitude immediately after the SH mode arrival is taken as a measure of intensity.

The distance from the source to the detector, which is 36.06 mm for all values of φ, is far greater than the dominant wavelengths of the signal at ultrasonic frequencies and therefore corresponds to the far field condition. In the far field of an isotropic medium, the theoretical intensity radiation pattern $I(\varphi)$ of the SH mode displacement polarized perpendicular to the sagittal plane is given by [7]

$$I(\varphi) \propto F^2(t)\cos^2\varphi/(\mu^2 R^2), \tag{5}$$

where μ is the shear modulus of an isotropic medium, R is the source-to-detector distance, and $F(t)$ is the time function of the SH mode source strength. Eq. (5) predicts a behavior of SH radiation pattern similar to Fig. 5 and indicates that for small values of φ, the intensity variation is proportional to φ^2 and very small. This behavior is in sharp contrast to the SH mode FT focusing pattern of the (001) silicon shown above, which indicates a drastic drop in intensity for a small range of φ due to a sharp focusing of the FT modes in silicon.

We now turn our attention to the determination of shear moduli from group velocity measurements. The measurement of C_{44} in silicon is already mentioned above. We used a transversely isotropic (hexagonal), 25. 7 mm thick disk of zinc oriented in the symmetry direction [001] and a 30 % weight carbon-fiber (CF) reinforced PEEK plate of 3.26 mm thickness. The thickness direction of PEEK and the [001] in zinc are denoted as the x_3 direction. The densities of zinc and PEEK are 7134 kg/m^3 and 1400 kg/m^3, respectively. The arrangement of the S-mode PZT source and detector is identical to that used with the silicon specimen, excepting that a line source (LS) type S-mode PZT source with a 5 mm long and 0.75 mm wide active element polarized in the 5 mm direction is used with the PEEK specimen.

For the transversely isotropic zinc, the (100) is identical with any zonal plane passing through the [001] axis. Because of the thick zinc disk, the detector position belongs to a far field. The signal observed is somewhat similar to the signal of x = 0 mm in

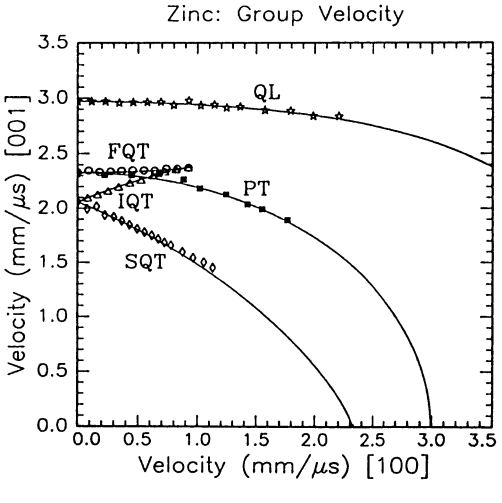

Figure 6. Measured group velocities in the zonal plane of zinc. Theoretical group velocity sections are juxtaposed.

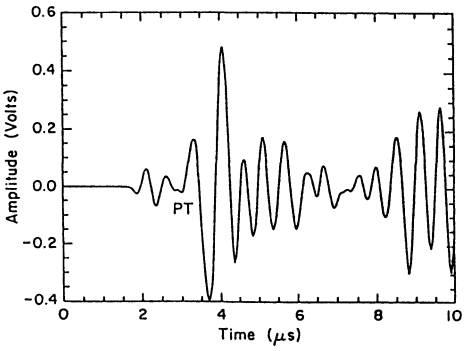

Figure 7. A typical off-epicentral SH signal detected by the S-mode PZT detector in the x_2x_3 plane of the PEEK plate. A line type S-mode PZT source is used at origin.

Fig. 2 and the SH mode PT arrival is found at the point at which the signal exceeds first the noise level. The measured SH polarized PT group velocities along several directions in the zonal plane are plotted in Figure 6 with the square symbols, together with other measurements for reference. The two shear moduli of zinc, $C_{44} = C_{55} = 38.8$ GPa and $C_{66} = (C_{11} - C_{12})/2 = 63.2$ GPa, are obtained using the least squares fit to these measurements.

For the orthorhombic PEEK, because of a rather thin thickness (3.26 mm), the detector position belongs to a near-field and the signal, which follows the QL arrival and precedes the PT arrival, is observed in the detected waveform shown in Figure 7. However, as the detector is rotated at the same position, the portion of the signal following the PT arrival exhibits a large swing in amplitude. PT arrival is determined at the point of beginning of this large swing and indicated in Fig. 9. Three shear moduli $C_{44} = 2.23$ GPa, $C_{55} = 2.41$ GPa, and $C_{66} = 5.71$ GPa are obtained from the arrival times of the SH PT waves propagating in the x_2x_3 and x_2x_3 planes. Because a rather short source-to-detector distance, the aperture effects of the finite size of the source and detector are substantial. As a result, the measured shear moduli of the PEEK are subjected to an error as large as 20 %. For detailed description of group velocity measurements in zinc and PEEK, refer to the papers of Kim et al. [8,9]

ACKNOWLEDGMENT

K.Y. Kim and W. Sachse acknowledge the financial support from the Office of Naval Research. R. Baker appreciates the support of the Materials Science Center of Cornell University, maintained through grants from the National Science Foundation.

REFERENCES

1. A.G. Every and K.Y. Kim, J. Acoust. Soc. Am. 95, 2505 (1994).
2. K.Y. Kim, Phys. Rev. 49, 3713 (1994).
3. K.Y. Kim, A.G. Every, and W. Sachse, J. Acoust. Soc. Am. 95, 1942 (1994).
4. J.A. Shields and J.P. Wolfe, Z. Phys. B 76, 11 (1989).
5. H.J. Maris, in *Nonequilibrium Phonons in Nonmetallic Crystals*, eds. W. Eisenmenger and A.A. Kaplyanskii (North-Holland, Amsterdam, 1986). pp. 51-91.
6. R.L. Weaver, M.R. Hauser, and J.P. Wolfe, Z. Phys. B 90, 27 (1993).
7. K. Aki and P.G. Richards, *Quantitative Seismology* (Freeman, San Francisco, 1970), Vol. 1.
8. K.Y. Kim, R. Sribar, and W. Sachse, J. Appl. Phys. 77, 5589 (1995)
9. K.Y. Kim, T. Ohtani, A.R. Baker, and W. Sachse, Res. Nondest. Eval. (in press).